EUROFUSION WPS2-PR(15) 14648

J M Faustin et al.

Fast particle loss channels in Wendelstein 7-X

Preprint of Paper to be submitted for publication in Nuclear Fusion

This work has been carried out within the framework of the EUROfusion Consortium and has received funding from the Euratom research and training programme 2014-2018 under grant agreement No 633053. The views and opinions expressed herein do not necessarily reflect those of the European Commission.

This document is intended for publication in the open literature. It is made available on the clear understanding that it may not be further circulated and extracts or references may not be published prior to publication of the original when applicable, or without the consent of the Publications Officer, EUROfusion Programme Management Unit, Culham Science Centre, Abingdon, Oxon, OX14 3DB, UK or e-mail Publications.Officer@euro-fusion.org

Enquiries about Copyright and reproduction should be addressed to the Publications Officer, EUROfusion Programme Management Unit, Culham Science Centre, Abingdon, Oxon, OX14 3DB, UK or e-mail Publications.Officer@euro-fusion.org

The contents of this preprint and all other EUROfusion Preprints, Reports and Conference Papers are available to view online free at http://www.euro-fusionscipub.org. This site has full search facilities and e-mail alert options. In the JET specific papers the diagrams contained within the PDFs on this site are hyperlinked

Fast particle loss channels in Wendelstein 7-X

J.M. Faustin[1], W.A. Cooper[1], J.P. Graves[1], D. Pfefferlé[1] and J. Geiger[2]

[1]Ecole Polytechnique Fédérale de Lausanne (EPFL), Swiss Plasma Center (SPC), CH-1015 Lausanne, Switzerland
[2]Max-Planck Institut für Plasmaphysik, D-17491 Greifswald, Germany

Abstract

One of the main goals of Wendelstein 7-X (W7-X) is to demonstrate the fast particle confinement properties of the quasi-isodynamic stellarator concept. Fast particle populations will be produced either by Neutral Beam Injection (NBI) or by minority Ion Cyclotron Resonant Heating (ICRH). A fraction of these particles are expected to be lost (even without collisions), despite the optimisation procedure used for the W7-X design. Confinement properties of NBI particles in W7-X were presented in the paper of M. Drevlak et al *Nucl. Fusion* 2014. A detailed study is presented here where the loss patterns of an NBI population are described. In particular, focusing on a high-mirror equilibrium, the confinement of fast ions with varying energy injection is studied under collisional conditions. It is found that collisions are not only responsible for classical transport losses but also enhance drift induced losses caused by the finite orbit width of trapped particles. Moreover, an asymmetry is found in the toroidal position of particle losses which can be explained by local variation in the equilibrium field. The effects of a neoclassically resolved radial electric field are also investigated. Fast particle confinement is significantly improved by the associated $\boldsymbol{E} \times \boldsymbol{B}$ drift. In particular, an increasing radial electric field helps to reduce and even stop the losses due the 3D equilibrium structure for times comparable to slowing down time.

1 Introduction

Wendelstein 7-X (W7-X) is a large superconductor stellarator presently under commissioning at IPP-Greifswald, Germany. One of the main objectives of this machine is to demonstrate the good confinement of fast ions in a quasi-isodynamic stellarator. In fusion reactors, alpha particles should provide a substantial source of plasma heating, and it is therefore essential to confine these particles over their slowing down time. The W7-X design was based, amongst other criteria, on an optimisation procedure aiming at good confinement of fast particles at high β. The experimental proof of the confinement capacity of a quasi-isodynamic stellarator therefore requires the generation of a fast particle population within 50keV to 100 keV and therefore the mechanisms responsible for losses of such particles in W7-X must be understood.

Losses of alpha particles will be of primary concern for a future fusion reactor. Of most concern will be of collsionless losses of particles still at, or near their birth energy. Monte Carlo simulations of alpha particles in quasi-isodynamic and quasi-symmetric configurations were first presented in Ref. [1] and showed that the quasi-isodynamic design appears to be the best candidate for a reactor design. Additional efforts for understanding the collisionless dynamics of fast ions in quasi-isodynamic equilibrium have been carried out. Losses induced by collisionless stochastic diffusion of fast ions was introduced in Ref. [1] and further developed in Ref. [2]. In addition, favourable conditions for unconfined collisionless orbits were discussed in Ref. [3]. The magnetic field curvature was shown to contribute significantly to the radial excursion of trapped particles. However, collisionality must also be considered in fast ion confinement studies since it is known to contribute to neoclassical transport of particles in general [4]. Recently, further numerical studies on fast ion confinement in W7-X configurations were presented in Ref. [5]. The latter work showed the effect of various magnetic equilibrium configurations on fast ions generated by neutral beam injection (NBI) at $\langle\beta\rangle = 2\%$. It was concluded that NBI may not be an efficient way to produce a fast particle population mostly because of rather poor beam penetration and rapid loss of injected particles. In the present paper, an understanding of the loss channels acting on a fast particle population produced by NBI is exposed. The particle guiding centre orbit solver VENUS-LEVIS and its dedicated NBI module [6] are

used to generate and evolve an NBI relevant population in a W7-X high mirror equilibrium. The distribution of lost particles is carefully analysed in order to identify the contribution of each of the loss channels previously discussed.

This paper is organised as follows. The MHD equilibrium used in this work is described in Section 2. The particle orbit classes and the bounce averaged motion of trapped particles in W7-X are discussed in Section 3. In Section 4, several particle loss channels are identified. NBI simulations with VENUS-LEVIS are described in Section 5. It is shown that mostly trapped particles are radially redistributed and potentially lost. In Section 6 the effects of a radial electric field on the fast particle orbits are described and it is shown that the particle confinement is significantly improved.

2 High-mirror equilibrium

W7-X has been optimised in part to confine energetic trapped particles over their slowing down time scale. Confinement is expected to be best for a high $\langle\beta\rangle$ MHD equilibrium. In such configurations, a given particle trapped in one of the five magnetic toroidal mirrors will mostly drift poloidally, the radial drift being low due to small geodesic curvature. The flexibility of the coil system on W7-X grants access to a broad range of magnetic equilibrium configurations, which are characterised by a mirror ratio value [5, 7] defined as :

$$mr = \frac{B_{\varphi=0} - B_{\varphi=\pi/5}}{B_{\varphi=0} + B_{\varphi=\pi/5}}. \quad (1)$$

A high-mirror magnetic configuration with $mr = 8.7\%$ was reconstructed by a fixed boundary equilibrium calculation using the VMEC/ANIMEC code [8, 9]. Poloidal cross sections of this equilibrium are displayed in Fig. 1 and show the toroidal variation of the equilibrium magnetic field amplitude. The central density and temperature were respectively set to $n_0 = 1.55 \times 10^{20} m^{-3}$ and $T_0 = 4keV$ in order to obtain a converged equilibrium with $\langle\beta\rangle = 4\%$.

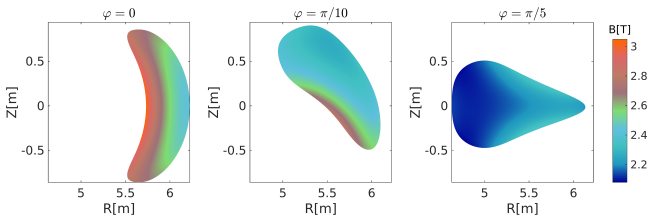

Figure 1 – Poloidal cross sections of W7-X equilibrium used. Colors indicate the amplitude of the equilibrium magnetic field.

3 Trapped particle precession drift in W7-X

The magnetic field inhomogeneities in magnetically confined fusion plasmas generate a diversity of particle trajectories. Classification of particle orbits has been carried out for tokamaks [10] and stellarators [11, 12]. In tokamaks, particle orbits fall into two main categories: passing and trapped. Depending on the magnetic field configuration trapped particle orbits may be characterised as banana, potato or tear drop type. In mirror machine type stellarators such as W7-X, a classification of the particle orbits can be made following the particle trajectory in a given toroidal period. If the particles parallel energy is sufficiently high it will overcome the local magnetic well and travel to the next toroidal period. Such particles are referred to as locally passing. The counterpart of this particle population are the locally trapped particles. More generally, particle orbits can be classified on the basis of their trajectory around the whole torus. The notion of critical magnetic field for particle reflection B_{ref} is introduced in order to understand this classification. This quantity defines the value that the ambient magnetic field must reach so that a particle is reflected. The particle energy E and magnetic magnetic moment μ, in the approximation of slowly varying fields, are constant along the free guiding centre trajectory. It is recalled:

$$E = \frac{1}{2} m \left(v_{\parallel}^2 + v_{\perp}^2 \right), \quad (2)$$

$$\mu = \frac{m v_{\perp}^2}{2B}. \quad (3)$$

If a particle is locally trapped then its parallel velocity $v_{\parallel}$ vanishes at the bounce points. B_{ref} is the magnetic field amplitude at the bounce point. Therefore the particle energy at this location is:

$$E = \frac{1}{2} m v_{\perp,bounce}^2 = \frac{1}{2} m v_{\perp,bounce}^2 \frac{B_{ref}}{B_{ref}} = B_{ref} \mu. \quad (4)$$

It then follows:

$$B_{ref} = \frac{E}{\mu}. \quad (5)$$

B_{ref} is a function of constants of motion, therefore it is suited to classify orbits in stellarators. The terminology introduced in Ref. [11] will be used. Three types of orbits are identified.

Passing particles: These particles are able to complete a full toroidal revolution around the machine without ever being reflected (assuming no collisions). Passing particles are characterised by a B_{ref} value higher than the maximum value of the equilibrium magnetic field on the particle trajectory.

Localised or toroidally trapped particles: Depending on the mirror ratio value, there can exist a population of particles that will remain locally trapped by the toroidal magnetic mirror and can never travel to the next toroidal period. In this case, the particle trajectory is toroidally bounded by two isosurfaces $B = B_{ref}$. These isosurfaces are poloidally closed and are located between two consecutive bean shaped cross sections in the case of W7-X.

Blocked or helically trapped particles: These particles are located in the region of phase space near the locally trapped-passing boundary. These particles may be regarded as locally trapped for a few bounces but they are able to de-trap collisionlessly. A blocked particle's trajectory is not restricted to a single toroidal segment but extends to neighbouring sections. Such particles are also called transitioning [2]. An illustration of these three types of orbits and a comparison with particle orbits in an axisymmetric plasma is given in Fig. 2. Orbits are drawn in a full torus and in a poloidal cross section.

In stellarators, the confinement of energetic trapped particles is of special concern because their radial drift may cause them to escape the last closed flux surface (LCFS) before de-trapping occurs. For thermal particles the collision frequency would be sufficiently high to de-trap particles and change their orbit topology to a confined configuration. However since the typical collision time of fast particles like alphas in a reactor is large compared to their confinement time, their confinement mainly relies on minimising the bounce averaged radial drift. The drift optimisation is based on the calculation of the longitudinal adiabatic invariant $\mathcal{J}$. This quantity is a function of phase space and one way to represent it is to consider the radial and poloidal locations (ψ_b, θ_b) of the bounce or transit points for fixed E and B_{ref}:

$$\mathcal{J}\left(\psi_b, \theta_b, E, B_{ref}\right) = \oint v_{\parallel} \mathrm{d}l. \tag{6}$$

where the integral path is taken along a particles complete bounce(trapped) or transit(passing) trajectory. This quantity can also be expressed in the magnetic coordinate system (ψ, θ, φ) using an adiabatic expansion:

$$\mathcal{J}\left(\psi_b, \theta_b, E, B_{ref}\right) \simeq \mathcal{J}_0\left(\psi_b, \theta_b, E, B_{ref}\right) \tag{7}$$

As in Ref [12], at the lowest order in the guiding center approximation, $\mathcal{J}$ is more conveniently calculated along the field line path. In an action-angle variable formalism, $\mathcal{J}_0$ contains information such as the bounce or transit time, but also the radial and poloidal deviation of the bounce or transit points from the field line. Therefore the bounce or transit time is simply:

$$T = \frac{\partial \mathcal{J}_0}{\partial E}. \tag{8}$$

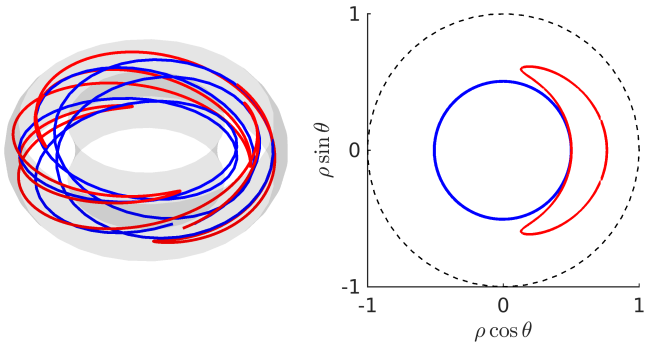

(a) Passing (blue) and trapped (red) particles orbit in an axisymmetric equilibrium

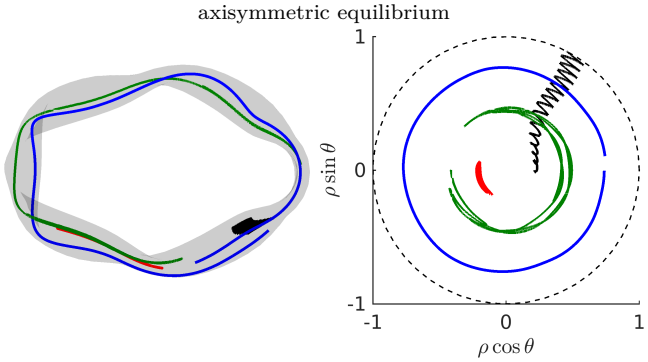

(b) Passing (blue), blocked (green) and localised (red) particles orbit in a W7-X high-mirror equilibrium. An unconfined deeply trapped particle orbit is shown in black.

Figure 2 – Examples of the main orbit topologies in an axisymmetric versus a W7-X high-mirror equilibrium. The dashed line represents in each case the last closed flux surface. $\rho = \sqrt{\Phi_{tor}/\Phi_{tor,edge}}$ and corresponds to a radial variable.

The change in the variable ψ and θ after a complete bounce or a transit are then respectively:

$$\Delta\psi = \oint_{bounce} \mathrm{d}\varphi \frac{\mathrm{d}\psi}{\mathrm{d}\varphi} = \frac{\partial \mathcal{J}_0}{\partial \theta}, \tag{9}$$

$$\Delta\theta = \oint_{bounce} \mathrm{d}\varphi \frac{\mathrm{d}\theta}{\mathrm{d}\varphi} = -\frac{\partial \mathcal{J}_0}{\partial \psi}. \tag{10}$$

The average radial and poloidal drift over a periodic motion straightforwardly reads:

$$\langle \dot{\psi} \rangle = \frac{\Delta\psi}{T} = -\frac{\frac{\partial \mathcal{J}_0}{\partial \theta}}{\frac{\partial \mathcal{J}_0}{\partial E}}, \tag{11}$$

$$\langle \dot{\theta} \rangle = \frac{\Delta\theta}{T} = -\frac{\frac{\partial \mathcal{J}_0}{\partial \psi}}{\frac{\partial \mathcal{J}_0}{\partial E}}. \tag{12}$$

In an optimised stellarator such as W7-X, the longitudinal adiabatic invariant is almost a flux surface quantity for most of the trapped particles: $\frac{\partial \mathcal{J}_0}{\partial \theta} \simeq 0$. Therefore the radial drift along the bounce averaged motion of trapped particles vanishes to lowest order. In this approximation these particles mostly drift poloidally and

remain confined on time scales larger that the typical slowing down time. In W7-X, drift optimised magnetic configurations are ensured by high thermal pressure. The expression for $\mathcal{J}_0$ for trapped particles is:

$$\begin{aligned}\mathcal{J}_0 &= \oint_{bounce} mv_\parallel \mathrm{d}l_f \\ &= \sqrt{2mE}\oint_{bounce}\sqrt{1-\frac{B}{B_{ref}}}\mathrm{d}l_f. \end{aligned} \tag{13}$$

Here $\mathrm{d}l_f$ is an infinitesimal field line element length which can be written from the field line equation:

$$\frac{\mathrm{d}l_f}{B} = \frac{\mathrm{d}\varphi}{\boldsymbol{B}\cdot\nabla\varphi}. \tag{14}$$

As the toroidal magnetic flux is given by:

$$\Phi_{tor}(\rho) = \int_{\rho'=0}^{\rho'=\rho}\int_{\theta=0}^{\theta=2\pi}\int_{\varphi=0}^{\varphi=2\pi}\sqrt{g}\boldsymbol{B}\cdot\nabla\varphi \mathrm{d}\rho'\mathrm{d}\theta\mathrm{d}\varphi, \tag{15}$$

in a straight field line flux coordinate system, the field line element length reads:

$$\mathrm{d}l_f = \sqrt{g}B\frac{\mathrm{d}\varphi}{\Phi'_{tor}}. \tag{16}$$

It then follows:

$$\mathcal{J}_0 = \sqrt{2mE}\oint_{bounce}\sqrt{1-\frac{B}{B_{ref}}}\sqrt{g}B\frac{\mathrm{d}\varphi}{\Phi'_{tor}} \tag{17}$$

$$= 2\sqrt{2mE}\int_{\varphi_1}^{\varphi_2}\sqrt{1-\frac{B}{B_{ref}}}\sqrt{g}B\frac{\mathrm{d}\varphi}{\Phi'_{tor}}. \tag{18}$$

where φ_1 and φ_2 are the toroidal position of the bounce points. From this expression it is possible to numerically evaluate the contours of $\mathcal{J}_0$ for different $\langle\beta\rangle$ and for $B_{ref} = 2.42T$ for the high mirror configuration described in the previous section. Fig. 3 shows the poloidal closure of $\mathcal{J}_0$ over most of the cross section for $\langle\beta\rangle = 4\%$ which leads to a reduction of trapped particle radial drifts. $\langle\beta\rangle = 1\%$ shows poor closure of $\mathcal{J}_0$. However it is impossible to ensure poloidal closure of $\mathcal{J}$ for all ranges of trapped particles, and over the entire plasma volume. As a consequence particle loss channels still exist and are described in the next section.

4 Loss channels

4.1 Stochastic diffusion losses

Stochastic diffusion of fast ions in optimised stellarators has been described in [2]. This diffusion process concerns transitioning particles, described in 3. The

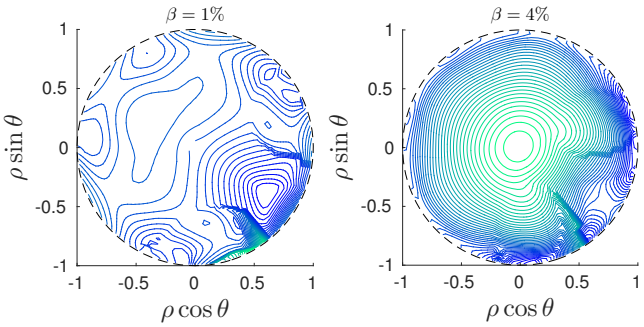

Figure 3 – Contours of constant $\mathcal{J}_0$ for $B_{ref} = 2.42T$ and two values of $\langle\beta\rangle$.

stochastic diffusion mechanism is as follows: a particle is able to change its orbit class (locally passing to locally trapped or vice-versa) if it crosses the phase-space separatrix between libration (locally trapped) and rotation (locally passing). This separatrix crossing implies a non adiabatic change in the particle motion [13]. However, an adiabatic treatment of the particle motion is still valid as long as the particle remains sufficiently far from the separatrix. In that case the particle motion can still be characterised by a parallel adiabatic invariant $\mathcal{J}$ during both the locally trapped and the locally passing motion. After multiple separatrix crossings, the adiabatic invariant associated with, for instance, the libration motion accumulates random jumps $\Delta\mathcal{J}$ which ultimately causes a stochastic diffusion in $\mathcal{J}$-space. In Ref [2] it was noted that each jump in $\mathcal{J}$ causes a radial displacement $\Delta\psi = \Delta\mathcal{J}\frac{\partial\psi}{\partial\mathcal{J}}$. This associated radial diffusion time is usually rather long compared to other loss mechanisms. Therefore it is expected that stochastic radial diffusion will account for losses of initially well confined weakly collisional transitioning fast particles.

4.2 Drift induced losses

Inspection of eqs. (11) and (12) shows that reducing trapped particle losses can be achieved by ensuring that these particles avoid regions where $\langle\dot{\psi}\rangle$ is enhanced compared to $\langle\dot{\theta}\rangle$. The unfavourable regions can be identified in terms of equilibrium parameters. Considering no radial electric field and a static equilibrium field, the guiding centre of a particle of mass m and charge q will drift perpendicularly to the magnetic field line with a drift velocity:

$$\boldsymbol{v_D} = \mathbf{b}\times\left(\frac{\mu}{q}\nabla B + v_\parallel\rho_\parallel B\boldsymbol{\kappa}\right)/B^*_\parallel. \tag{19}$$

Where $\rho_\parallel = mv_\parallel/qB$, $\boldsymbol{b} = \boldsymbol{B}/B$, $B^*_\parallel = \boldsymbol{b}\cdot\left(\boldsymbol{B}+\rho_\parallel\nabla\times\boldsymbol{B}\right)$ and $\boldsymbol{\kappa} = -\boldsymbol{b}\times(\nabla\times\boldsymbol{b})$ is the magnetic field line curvature. The latter can be used to relate the

equilibrium configuration to the particle losses pattern. The field lines lie on curved magnetic flux surfaces, and in particular [14], the field line curvature is composed of a normal and a geodesic curvature. The field line curvature can be written :

$$\boldsymbol{\kappa} = \kappa_n \frac{\nabla s}{|\nabla s|} + \kappa_g \frac{\boldsymbol{B} \times \nabla s}{|\boldsymbol{B} \times \nabla s|}. \tag{20}$$

Where $s = \Phi_{tor}/\Phi_{tor,edge}$ is a flux surface label and serves as radial coordinate in the magnetic coordinate system (s, θ, φ). From the definition of $\boldsymbol{\kappa}$ and assuming MHD force balance and nested flux surfaces, one can show that:

$$\boldsymbol{\kappa} = \frac{\nabla_\perp B}{B} + \mu_0 \frac{p' \nabla s}{B^2}, \tag{21}$$

with $p' = \frac{\mathrm{d}p}{\mathrm{d}s}$, so that the bounce averaged radial drift depends only on κ_g:

$$\oint_{bounce} \boldsymbol{v_D} \cdot \frac{\nabla s}{|\nabla s|} \mathrm{d}t = \oint_{bounce} -\left(\frac{\mu}{q} + v_\parallel \rho_\parallel\right) \frac{B}{B^*_\parallel} \kappa_g \mathrm{d}t, \tag{22}$$

$$\kappa_g = \frac{1}{\sqrt{g} B^2 \sqrt{g^{ss}}} \left(\frac{\partial B}{\partial \theta} B_\varphi - \frac{\partial B}{\partial \varphi} B_\theta\right). \tag{23}$$

It appears clearly (as is well known) that particles with bounce trajectories mostly located in regions with negative geodesic curvature drift radially outwards and eventually escape the plasma. Examples of such unconfined orbits are illustrated in Fig. 4. There are various types of "bad" curvature regions in W7-X. As seen in Fig. 4b, certain isosurfaces of B may exhibit narrow tubes with large radial extension and encapsulating a volume of negative curvature. In that case a trapped particle may fall into one of these tubes along its bounce trajectory and would quickly drift out of the plasma volume. Those tubes can be regarded as leaks in regions of phase space which mostly contain well confined particles. The avoidance of such tubes would mitigate this loss channel and might be worthwhile to be considered as an additional criterion in stellarator optimisation with respect to fast particle confinement.

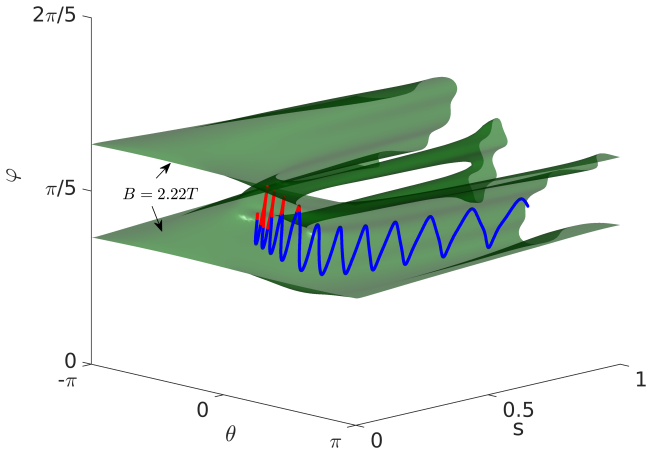

(a) Unconfined trapped particle running along lowest φ value of the $B_{ref} = 2.22T$.

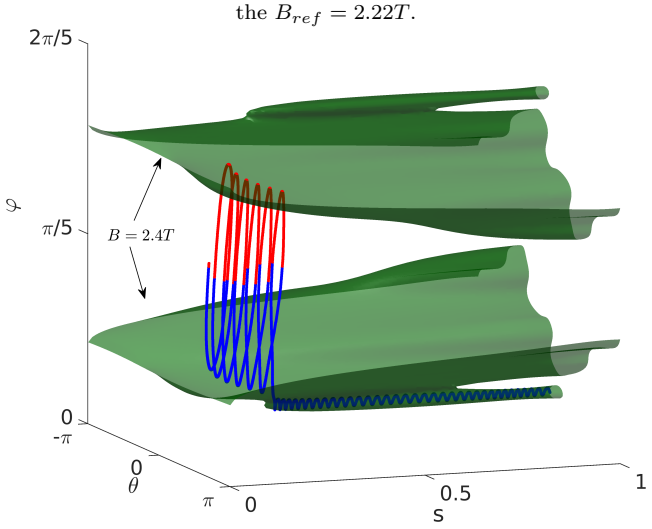

(b) Unconfined trapped particle running along lowest φ value of the $B_{ref} = 2.4T$ surface.

Figure 4 – Examples of unconfined localised particle orbits. The particle guiding centre drift trajectory is traced in each case and is seen to bounce between surfaces of constant $B = B_{ref}$. The color of the trajectory is representative of the local magnetic geodesic curvature sign (blue: $\kappa_g < 0$, red: $\kappa_g > 0$).

4.3 Effects of Coulomb collisions

In the presence of collisions, acting as pitch angle scattering as well as slowing down process, fast ions are expected to undergo collisional transport that redistributes them radially. Additionally, as fast ions slow down by colliding with the thermal ions and electrons, they also experience pitch-angle scattering. Therefore a rearrangement of the distribution of particles in phase space occurs that leads to collisional trapping and detrapping. Deeply trapped particles are expected to be generated by this process and before this particular fraction of the particle population can de-trap, they might

experience a significant net outward radial drift because of the mechanism described in the previous subsection. In that sense, collisions give favourable conditions for drift induced losses. This mechanism will be clearly identified by simulations results in Section 5.

5 NBI simulations with VENUS-LEVIS

In this section, VENUS-LEVIS simulations of fast ions generated by the dedicated NBI module [6] are presented. The simulated particles are deuterium ions at 60keV, 30keV and 20keV. It is important to mention that it is not intended to model an NBI experiment which would involve continuous injection of fast ions. Instead, special attention is given to the dynamics of fast particles with energy representative of a neutral beam population. Furthermore, it is not intended that the model used should reproduce the W7-X NBI system in its exact geometry. However the injection angles were set so that the initial distribution in pitch-angle $\lambda = v/v_{||}$ is relevant with the normal and tangential PINIs injecting in the co- and counter direction with respect to the equilibrium toroidal magnetic field, as seen in Fig. 5a. An important feature of the initial population for the loss channel analysis is shown by the distribution in $\mu/E = 1/B_{ref}$ plotted in Fig. 5b: the fraction of deeply trapped particles, i.e. with $1/B_{ref} > 0.4$ is almost vanishing. It is reminded that the locally passing-trapping boundary depends on the considered drift surface. As the initial marker distribution spans radially across the whole plasma volume, it is not possible to identify a unique passing-trapped boundary. However, an adequate way to estimate the proportion of deeply trapped and deeply passing particles is to consider the inverse of the minimum and of the maximum of the magnetic field amplitude in the bean shaped cross section. These values are plotted in Fig. 5b by the two dotted lines. Collisional trapping effects described in 4.3 will be easily emphasised simply by comparing the initial and the final fraction of particles with $1/B_{ref} > 0.4$, i.e. $1/B_{ref} > 1/min_{\varphi=0}B$.

This marker population is evolved under slowing down and pitch angle scattering conditions. In VENUS-LEVIS these processes come from the interaction between the fast ions and the background species, i.e no self collisions of the fast ions are considered. The simulation comprises only the confined plasma volume, and as such a marker is recorded as lost as soon as it crosses the LCFS. Fig. 6 shows the cumulative number of lost markers over time. The loss history is similar for the three investigated initial energies. Markers that cross the LCFS before $t = 1$ms correspond to first orbit losses

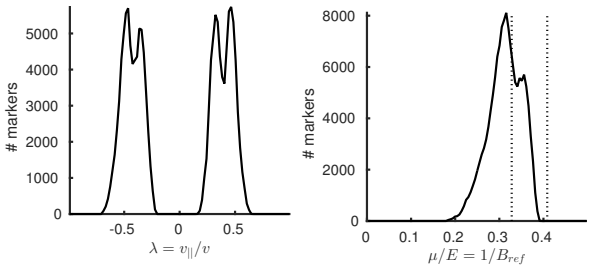

(a) (b)

Figure 5 – Initial pitch angle and $1/B_{ref}$ distribution. The dotted lines display the values corresponding to the minimum (left) and the maximum (right) of the magnetic field amplitude in the bean shaped cross section.

while losses after 1ms arise from a combination of the collisional and drift induced losses. The latter losses appear to be continuing steadily even after times comparable to the slowing down time of the fast ions. As we will see later, these thermalised particles are ultimately confined with the addition of a radial electric field. These distinct loss regimes can be also distinguished in Fig. 7 which displays the toroidal position at which a marker is lost with respect to its confinement time. These two types of losses are described separately.

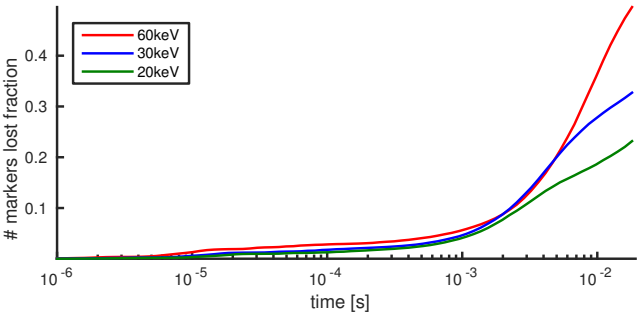

Figure 6 – Particle losses over time for different injected energy. Two loss regimes appear: first orbit losses (<1ms) and collisional/drift losses (>1ms).

First and multiple orbit losses. Fast particles born sufficiently close to the last closed flux surface and with a sufficiently large orbit width may escape the confined plasma volume during their bounce or transit motion. First orbit losses are observed when particles leave the confined volume before completing their bounce motion. In a mirror machine such as W7-X, one may also define multiple bounce (but early) losses since injected trapped particles can have a positive bounce average radial drift and leave the plasma only after bouncing a few times. First and multiple orbit losses can be seen by the stripe pattern in Fig. 7 and illustrated in Fig. 8. Multiple orbit losses are typical for stellarator machines and cannot

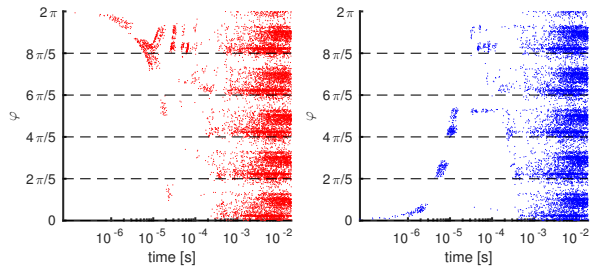

(a) 60 keV co-injected (b) 60 keV Counter-injected

Figure 7 – Toroidal position of lost markers over time in collisional conditions. First orbit losses clearly appear and display a different pattern for co- and counter- injected particles. After many bounce (or transit) times, the same loss pattern is observed in each toroidal period for a given energy injection. Dashed lines correspond to the boundaries between each toroidal period.

be observed in tokamaks because of the orbit symmetry.

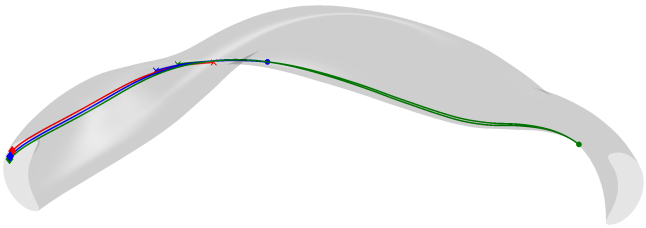

(a) First orbit losses

(b) multiple orbit losses

Figure 8 – Example of first and multiple orbit losses. ⧫: initial positions, •: bounce tips, ×: lost positions.

Collisional and drift induced losses. Coulomb collisions with the thermal ions and electrons will not only be responsible for slowing down of particles but also for pitch angle scattering. Therefore collisions can be considered as a source of particle trapping and de-trapping. It is recalled that the fraction of initially deeply trapped particles is nearly vanishing, but as seen in Fig. 9 the population of particles lost after 1ms consists mostly of trapped particles. Indeed, particles that can be identified as being in a deeply trapped state and being lost after 1ms represent 53% of the total number of losses after that time (the second peak on the dash-dotted line in Fig. 9). This means that not only will particles undergo collisional transport (diffusion in position space) but also wander in and out of the trapped region of phase space via pitch angle scattering (diffusion in velocity space). During the time in which particles remain deeply trapped they experience a net outward radial drift as described in 4.2. Additionally, the two peaks in Fig. 9 are retrieved at particular toroidal positions in Fig. 7 where dense clouds of points are observed in particular locations of each toroidal segment. These locations corresponds to local magnetic wells in which particles are locally trapped due to collisions and where they drift out until they exit the plasma. The losses located in the middle of each toroidal segment can be explained by the local magnetic variation around the triangle cross section as seen in Fig. 1. A second loss region appears at the entry of the toroidal segments. However, by virtue of the stellarator symmetry [15], local magnetic wells that are found around a (θ, φ) region appear also around $(-\theta, -\varphi)$ since:

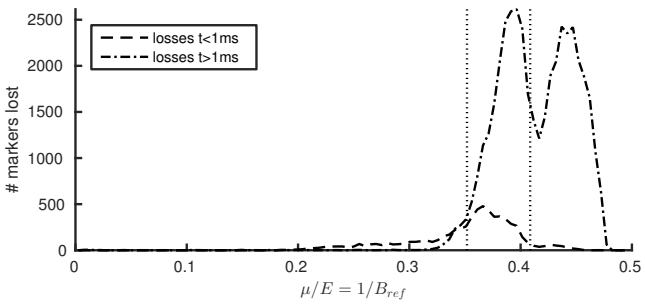

Figure 9 – Particle losses as a function of their pitch angle variable μ/E.

$$I_0 B\left(\rho, \theta, \phi\right) = B\left(\rho, -\theta, -\phi\right), \tag{24}$$

where I_0 is the symmetry operator defined in Ref. [15]. This operator transforms the covariant components of $\boldsymbol{B}$, since it is a stellarator symmetric vector field as follow:

$$I_0\left[B_s, B_\theta, B_\varphi\right] = \left[-I_0 B_s, I_0 B_\theta, I_0 B_\varphi\right]. \tag{25}$$

Partial derivatives are transformed as:

$$I_0\left[\frac{\partial}{\partial s}, \frac{\partial}{\partial \theta}, \frac{\partial}{\partial \phi}\right] B = \left[\frac{\partial}{\partial s}, -\frac{\partial}{\partial \theta}, -\frac{\partial}{\partial \phi}\right] I_0 B, \tag{26}$$

It then follows from (23),(25) and (26) that the geodesic curvature transforms under stellarator symmetry into:

$$\kappa_g\left(s, \theta, \varphi\right) = -\kappa_g\left(s, -\theta, -\varphi\right). \tag{27}$$

Hence, the toroidal asymmetry in the loss pattern can be explained by the changed sign of the geodesic curvature when moving from a local magnetic well location to its sellarator symmetric location. This is confirmed in Fig. 10 which shows the geodesic curvature map on the LCFS and the contours of $1/B$.

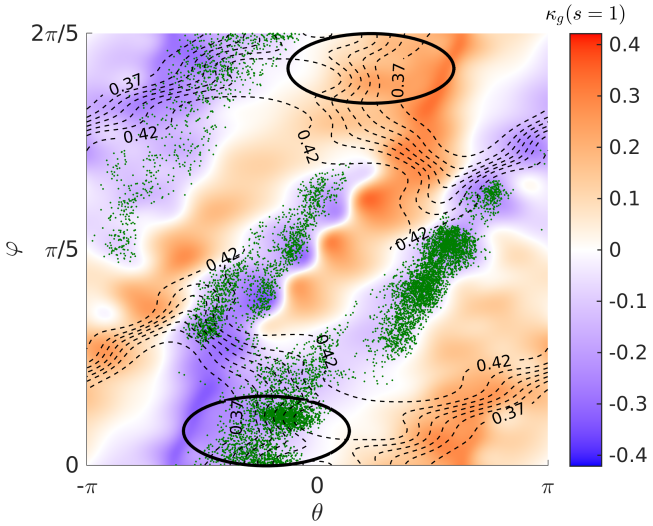

Figure 10 – Lost particles position in a chosen toroidal segment in the $\theta - \varphi$ plane (green dots). Circles emphasise stellarator symmetric local magnetic wells. Colors show the geodesic curvature amplitude on the LCFS.

6 Effects of a radial electric field

In this section, the effects of a neoclassically resolved radial electric field are investigated. A radial electric field (E_r) arises from the ambipolarity condition for the neoclassical particle transport of background electrons and ions adding a predominantly poloidal $\boldsymbol{E}\times\boldsymbol{B}$ drift to the particles motion. Therefore it is expected that such an electric field will increase the poloidal drift motion of trapped particles and improve their confinement. The $\boldsymbol{E}\times\boldsymbol{B}$ induced velocity drift reads as:

$$\begin{aligned}\boldsymbol{v}_{\boldsymbol{E}\times\boldsymbol{B}} &= \frac{\boldsymbol{E}\times\boldsymbol{b}}{B^*_\parallel} \\ &= \frac{E_r}{|\nabla s| B B^*_\parallel \sqrt{g}} \left(B_\theta \boldsymbol{e}_\varphi - B_\varphi \boldsymbol{e}_\theta\right) \end{aligned} \tag{28}$$

Inspection of eqs. (28) and (19) indicates that the improvement in the particle confinement by the $\boldsymbol{E}\times\boldsymbol{B}$ poloidal drift is less effective for high energy particles. The radial electric field profile used in the following corresponds to the so-called ion-root regime [16] and is displayed in Fig. 11a. Fig. 11b shows an example of how the inclusion of $\boldsymbol{v}_{\boldsymbol{E}\times\boldsymbol{B}}$ helps to confine a trapped particle that would otherwise escape the plasma if only the drifts (19) are resolved. The same initial fast ion population as in the previous section was evolved in the presence of this radial electric field. A scan in the radial electric field amplitude was performed in order to analyse its effect on the fast ion confinement. Fig. 12 shows the particle loss fraction over time with varying radial electric field amplitude and initial energy (left to right). Here 100% E_r is the correct level of radial electric field according to neoclassical calculations. It is seen that the fast ion confinement is strongly enhanced. More precisely the number of lost particles saturates with time for a sufficiently high electric field amplitude. In particular, as expected, 20keV ions experience a larger enhancement in their confinement, and for a realistic electric field amplitude the losses due to the 3D equilibrium configuration stop over times comparable with the particles slowing down time.

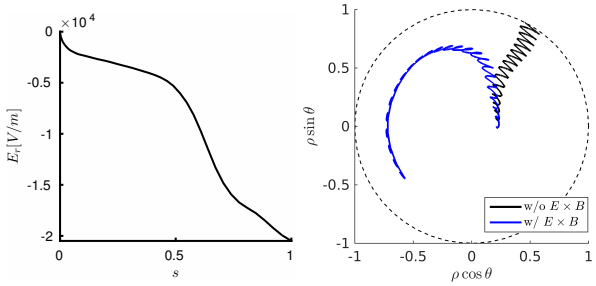

(a) Radial electric profile E_r resolved by neoclassical calculation.

(b) Confinement effect due to the $\boldsymbol{v}_{\boldsymbol{E}\times\boldsymbol{B}}$.

Figure 11 – Radial electric field profile and its effect on a trapped particle orbit.

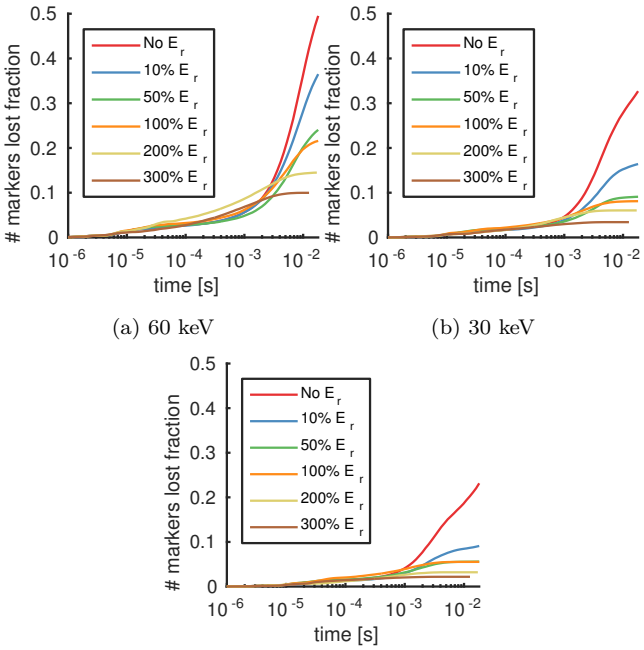

(a) 60 keV

(b) 30 keV

(c) 20 keV

Figure 12 – Particle lost fraction over time for various radial electric field amplitude and injection energy: a)60 keV, b)30 keV, c)20 keV.

Furthermore, the radial deposition profile of the in-

jected fast ions is affected by the inclusion of E_r. As seen in Fig. 13, for larger electric fields the distribution is more peaked in the central region. Moreover, the edge distribution tends to drop with increasing E_r because of the reduced radial transport. Figs. 12 and 13 show a strong influence of the radial electric field on the fast ions dynamics in W7-X plasmas. As a concluding remark of this section, it should be stated that future studies concerning fast ions confinement and generation (in particular in W7-X) should include a realistic equilibrium radial electric field.

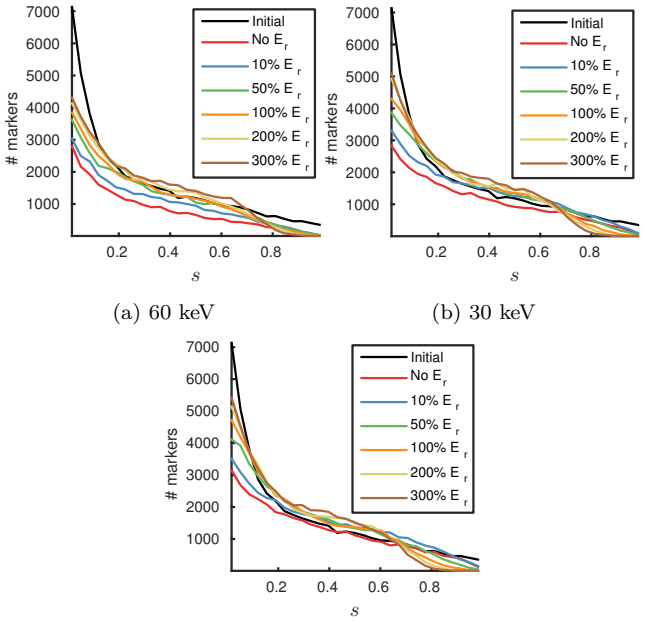

(a) 60 keV (b) 30 keV

(c) 20 keV

Figure 13 – Radial deposition profile for various injection energy and radial electric field amplitude.

Summary and conclusions

The work presented here shows the particle loss patterns that are expected at neutral beam injection (NBI) relevant energies and pitch angles. Fast particle loss channels have been identified. First the stochastic radial diffusion described in Ref. [2] is expected to play a significant role for high energy (i.e. low collisional) particles confined for a long time. Earlier losses can be split into two regimes. The first one involves first and multiple orbit losses. The second regime is explained by a drift induced loss mechanism. In this regime, Coulomb collisions will cause classical transport but more importantly will generate deeply trapped particles via pitch angle scattering. Trapped particles generated by this scattering process are mostly transported outside the plasma by the drift induced loss channel. The effects of the ambipolar radial electric field which has been derived from neoclassical transport simulations have been described. Fast ion confinement is noticeably improved in the considered range of energies. It was observed that the $\boldsymbol{v}_{\boldsymbol{E}\times\boldsymbol{B}}$ drift essentially prevent the losses due to the 3D magnetic equilibrium properties ($|B|$ and curvature distribution) for particles slowing down from an injection energy of 60keV. The neoclassically determined radial electric field is just sufficient to provide good confinement of such a population. The inclusion of these effects may help the numerical development of fast ion generation scenarios for W7-X. In particular, it is foreseen fast ion generation scenarios involving minority Ion Cyclotron Resonant Heating (ICRH) would benefit from the $\boldsymbol{E}\times\boldsymbol{B}$ effect. Indeed, minority ICRH is based on building a fast ion tail from a thermal ion population. The radial electric field should enable the confinement of ions for sufficient time for ICRH to energise the particles. However, ICRH enhances the ion velocity dominantly in the perpendicular direction. For the plasmas analysed in this paper, the resulting trapped ions cannot be expected to reach temperatures beyond around 50keV where the benefits of the radial electric field become weak.

Acknowledgments

The authors would like to thank C. D. Beidler, M. Drevlak, P. Helander, J. Dominski and S. Lanthaler for insightful discussions. The authors are also grateful to D. Moseev and Yu. Turkin for providing the radial electric field profile.

This work has been carried out within the framework of the EUROfusion Consortium and has received funding from the Euratom research and training programme 2014-2018 under grant agreement No 633053. The views and opinions expressed herein do not necessarily reflect those of the European Commission. The project was also supported in part by the Swiss National Science Foundation. The authors thank Dr. S. P. Hirshman for providing us with the VMEC code. Much of the numerical work was performed at the CSCS, Lugano, Switzerland, at the IFERC, Rokkasho, Japan. This work was supported by EPFL through the use of the facilities of its Scientific IT and Application Support Center.

References

[1] W Lotz, P Merkel, J Nuehrenberg, and E Strumberger. Collisionless alpha -particle confinement in stellarators. *Plasma Phys. Control. Fusion*, 34(6):1037–1052, 1992.

[2] C. D. Beidler, Ya. I. Kolesnichenko, V. S. Marchenko, I. N. Sidorenko, and H. Wobig. Stochastic diffusion of energetic ions in optimized stellarators. *Phys. Plasmas*, 8(6):2731, 2001.

[3] Horst Wobig. Theory of advanced stellarators. *Plasma Phys. Control. Fusion*, 41(3A):A159–A173, 1999.

[4] H. E. Mynick. Transport optimization in stellaratorsa). *Physics of Plasmas*, 13(5):–, 2006.

[5] M. Drevlak, J. Geiger, P. Helander, and Y. Turkin. Fast particle confinement with optimized coil currents in the W7-X stellarator. *Nucl. Fusion*, 073002, 2014.

[6] D. Pfefferlé, J.P. Graves, W.A. Cooper, C. Misev, I.T. Chapman, M. Turnyanskiy, and S. Sangaroon. Nbi fast ion confinement in the helical core of mast hybrid-like plasmas. *Nuclear Fusion*, 54(6):064020, 2014.

[7] J Geiger, H Maassberg, and C. D. Beidler. Investigation of Wendelstein 7-X Configurations with Increased Toroidal Mirror. *35th EPS Conference on Plasma Phys. Hersonissos*, 32D:5–8, June 2008.

[8] S. P. Hirshman. Steepest-descent moment method for three-dimensional magnetohydrodynamic equilibria. *Phys. Fluids*, 26(12):3553, 1983.

[9] W. a. Cooper, S. P. Hirshman, P. Merkel, J. P. Graves, J. Kisslinger, H. F G Wobig, Y. Narushima, S. Okamura, and K. Y. Watanabe. Three-dimensional anisotropic pressure free boundary equilibria. *Comput. Phys. Commun.*, 180(9):1524–1533, September 2009.

[10] L-G Eriksson and F Porcelli. Dynamics of energetic ion orbits in magnetically confined plasmas. *Plasma Phys. Control. Fusion*, 43(4):R145–R182, 2001.

[11] A Gibson and J B Taylor. Single Particle Motion in Toroidal Stellarator Fields. *Phys. Fluids*, 10(12):2653–2659, 1967.

[12] John R. Cary, C. L. Hedrick, and J. S. Tolliver. Orbits in asymmetric toroidal magnetic fields. *Phys. Fluids*, 31(6):1586, 1988.

[13] J. R. Cary, D.F. Escande, and J.L. Tennyson. Adiabatic-invariant change due to separatrix crossing. *Physical Review A*, 34(5), 1986.

[14] W. D'Haeseleer. *Flux coordinates and magnetic field structure: a guide to a fundamental tool of plasma structure.* Springer series in computational physics. Springer-Verlag, 1991.

[15] R.L. Dewar and S.R. Hudson. Stellarator symmetry. *Physica D: Nonlinear Phenomena*, 112(1–2):275 – 280, 1998. Proceedings of the Workshop on Time-Reversal Symmetry in Dynamical Systems.

[16] P Helander, C D Beidler, T M Bird, M Drevlak, Y Feng, R Hatzky, F Jenko, R Kleiber, J H E Proll, Yu Turkin, and P Xanthopoulos. Stellarator and tokamak plasmas: a comparison. *Plasma Phys. Control. Fusion*, 54(12):124009, December 2012.